Hydraulic transport across hydrophilic and hydrophobic nanopores: Flow experiments with water and *n*-hexane

Simon Gruener*
Experimental Physics, Saarland University, D-66041 Saarbrücken, Germany
and Sorption and Permeation Laboratory, BASF SE, D-67056 Ludwigshafen, Germany

Dirk Wallacher
Experimental Physics, Saarland University, D-66041 Saarbrücken, Germany
and Department Sample Environments, Helmholtz-Centre Berlin for Energy and Materials, Hahn-Meitner-Platz 1, D-14109 Berlin, Germany

Stefanie Greulich
Experimental Physics, Saarland University, D-66041 Saarbrücken, Germany

Mark Busch
Institute of Materials Physics and Technology, Eißendorfer Str. 42, D-21073 Hamburg-Harburg, Germany

Patrick Huber†
Experimental Physics, Saarland University, D-66041 Saarbrücken, Germany
and Institute of Materials Physics and Technology, Eißendorfer Str. 42, D-21073 Hamburg-Harburg, Germany
(Received 12 October 2015; published 4 January 2016)

We experimentally explore pressure-driven flow of water and *n*-hexane across nanoporous silica (Vycor glass monoliths with 7- or 10-nm pore diameters, respectively) as a function of temperature and surface functionalization (native and silanized glass surfaces). Hydraulic flow rates are measured by applying hydrostatic pressures via inert gases (argon and helium, pressurized up to 70 bar) on the upstream side in a capacitor-based membrane permeability setup. For the native, hydrophilic silica walls, the measured hydraulic permeabilities can be quantitatively accounted for by bulk fluidity provided we assume a sticking boundary layer, i.e., a negative velocity slip length of molecular dimensions. The thickness of this boundary layer is discussed with regard to previous capillarity-driven flow experiments (spontaneous imbibition) and with regard to velocity slippage at the pore walls resulting from dissolved gas. Water flow across the silanized, hydrophobic nanopores is blocked up to a hydrostatic pressure of at least 70 bar. The absence of a sticking boundary layer quantitatively accounts for an enhanced *n*-hexane permeability in the hydrophobic compared to the hydrophilic nanopores.

DOI: 10.1103/PhysRevE.93.013102

I. INTRODUCTION

Liquid flow and shear in pores a few nanometers across plays a dominant role in a plethora of processes and phenomena encompassing transport across biomembranes and biological tissues [1–3], geological erosion and hydraulic fracturing [4,5], the synthesis of nanostructured hybrid materials by electrodeposition [6] or melt infiltration [6–11], the separation of liquids by filter membranes, the durability of concrete [12–14], and friction [15–17]. The possibility for energy storage by forced liquid intrusion in nanoporous media is another topic which increasingly attracts interest both from a fundumental and an applied perspective [18–21].

Also the goal for an engineering of flows of minute amount of liquids in small devices, i.e., the design of laboratory-on-a-chip devices [1,22–41], motivates research activities with regard to the flow properties of liquids in extreme spatial confinement.

Similarly as for the thermodynamic equilibrium properties of pore-confined condensed matter [11,42–46], a couple of interesting questions regarding the transport behavior for the flow in such restricted geometries arise [47]: (i) Can the macroscopic wetting properties or values of fluid parameters, such as the viscosity η, surface, and interfacial tensions σ, accurately describe a liquid down to very small length scales, on the order of the size of its building blocks [36,48–50]? (ii) What happens with the conventional hydrodynamic no-slip shear stress boundary condition at the confining walls? (iii) How sensitive depends the nanofluidic transport behavior on dissolved gases?

Measurements with the surface-force apparatus (SFA), which allow one to study shear viscosities [51–57] and frictional properties [15–17] of thin films with thicknesses down to subnanometers, have revealed that, depending on the shear rate, the type of molecule, and the surface chemistry, sometimes remarkably robust bulk fluidity could be observed and sometimes also sizable deviations.

In general, the enormous academic and economic interests on the interfacial behavior of liquids are manifested by a vast publication rate concerning this issue during the past decade. Many different techniques like SFA, atomic force microscopy, particle image velocimetry, fluorescence recovery after photobleaching and controlled dewetting as well as

*simon-alexander.gruener@basf.com
†patrick.huber@tuhh.de

molecular dynamics or lattice Boltzmann simulations were utilized [36,58–62].

To date many factors have been found that seem to influence the boundary conditions. The most prominent and maybe the least controversially discussed among them is the fluid-wall interaction expressed in terms of the wettability [30,60,62–76]. The weaker the interaction the more likely the slip. In addition, shear rates beyond a critical value are supposed to induce slip, too [77–81]. In contrast, the influence of surface roughness is rather debatable [82]. There are results for a decrease [64,83] as well as for an increase [84] of the slip length with increasing surface roughness. Furthermore, dissolved gases [59,85–87], the shape of the fluid molecules [68], or the add-on of surfactants [88] seem to influence the boundary conditions. In summary, there is a huge set of factors (see Refs. [36,58,85,89]) and certainly a complex interplay among many of them that finally determines the interfacial flow behavior.

Pioneering experiments to probe transport behavior through nanoporous media were performed by Nordberg [90] and Debye and Cleland in the middle of the 1900s [91]. Nordberg studied water and acetone flow, whereas Debye and Cleland reported on the flow of a series of linear hydrocarbons (n-pentane to n-octadecane) through nanoporous Vycor glass. Flow rates in agreement with Darcy's law, the generalization of Hagen-Poiseuille's law for simple capillaries towards porous media [92], were observed.

As Abeles *et al.* [93] documented by an experimental study on toluene using also nanoporous Vycor glass, flow in nanoporous media can be through molecular flow (also termed Knudsen diffusion [94]), surface diffusion, and viscous liquid flow driven by capillary forces (termed "spontaneous imbibition") [92,95,96] or by external hydraulic pressure (called "forced imbibition") [97,98], depending on the size of the pores and on the temperature and pressure of the fluid.

In the following we focus on forced imbibition dynamics of water and n-hexane across monolithic Vycor glass monoliths with two distinct mean pore diameters. After a short introduction to flow across spongelike porous media, we present our experimental setup and discuss our results with regard to the hydrodynamic boundary conditions at the pore walls as a function of surface functionalization and the possible influence of dissolved gases.

II. PRINCIPLES OF LIQUID FLOWS IN A NANOPOROUS MEDIUM

The measurements presented below involve the flow of liquids through Vycor, a complex pore network comparable to a sponge. As simple approximation one can reduce the problem to the flow of a fluid through a tiny capillary. Consequently, the law of Hagen-Poiseuille is the starting point of the subsequent development of a theory of the liquid flow in a pore network.

A. Liquid flow in isotropic pore networks

For a given pressure difference Δp applied along a cylindrical duct with radius r and length ℓ the volume flow rate $\dot{V}$ is determined by

$$\dot{V} = \frac{\pi\, r^4}{8\,\eta\,\ell}\,\Delta p. \tag{1}$$

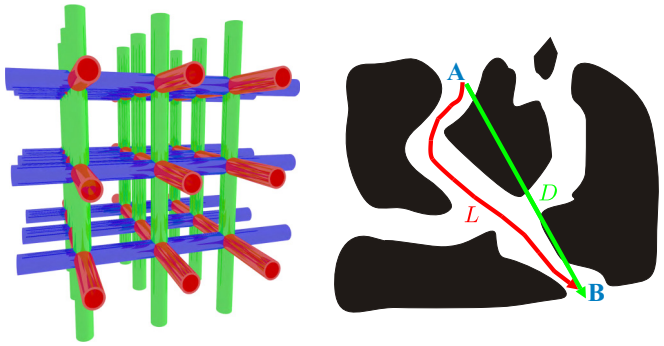

FIG. 1. Illustration of the meaning of the tortuosity τ of a pore network such as Vycor. Left: For an isotropic distribution of the pores only every third pore is subjected to the pressure gradient yielding $\tau = 3$. Right: For meandering pores an additional factor of $\frac{L}{D}$ must be introduced to correct the length D of the direct interconnection of two points for the actual path length L.

Here η denotes the dynamic viscosity of the flowing liquid. In the next step, one has to evolve concepts in order to account for the spongelike structure of an isotropic pore network. In general such a network can be characterized by three quantities. The mean pore radius r_0 and the volume porosity ϕ_0, as obtained from sorption isotherm experiments, are probably the most intuitive ones among them. With only these two parameters a porous cuboid with edge length a (and cross-sectional area $A = a^2$) consisting of

$$n = \frac{\phi_0\, A}{\pi\, r_0^2} \quad \left(\Leftrightarrow \phi_0 \equiv \frac{V_{\text{void}}}{V_{\text{sample}}} = \frac{n\,\pi\, r_0^2\, a}{a^3} \right) \tag{2}$$

cylindrical pores with radius r_0 and length a can be constructed. Assuming the capillaries to be aligned in flow direction the flow rate through the whole matrix is then given by n times the single pore flow rate Eq. (1) with $r = r_0$ and $\ell = a$. However, so far this description still lacks information on the orientation of the pores.

To account for the isotropy of the network as indicated in Fig. 1 (left) it is necessary to introduce a third parameter, the so-called tortuosity τ, along with the transformation

$$\dot{V} \longrightarrow \frac{1}{\tau}\dot{V} \tag{3}$$

of the volume flow rate Eq. (1). Pores totally aligned in the flow direction would yield $\tau = 1$, whereas isotropic distributed pores would result in $\tau = 3$. For a random orientation only every third pore is subjected to the pressure gradient and hence contributes to the flow. Therefore, the net flow rate has to be divided by the factor three. But no correction is needed if all pores are aligned in flow direction and as a result of this it is $\tau = 1$. In this way the tortuosity is a simple method for accounting for the orientation of the pores with respect to the direction of the pressure drop.

To date several techniques have been applied to extract the tortuosity of the isotropic pore network in Vycor glass. Deducing the diffusion coefficient of hexane and decane by means of small-angle neutron-scattering (SANS) measurements τ was found to be in the range of 3.4–4.2 [99]. Gas permeation measurements performed with an in-house apparatus resulted

in $\tau = 3.9 \pm 0.4$ [94,100]. Finally, calculations based on three-dimensional geometrical models yielded a value of approximately 3.5 [101].

Interestingly, all values show a significant deviation from $\tau = 3$ as derived from the previous considerations. Accordingly, there must be an additional aspect of the geometry that has so far been neglected. Regarding Fig. 1 (right) this issue is apparent: The pores are not straight but rather meandering. In consequence, the length L of the path from any point A to another point B is always larger than the length D of the direct interconnection of the two points. To correct the pore length for the larger flow path an additional factor of $\frac{L}{D}$ for the tortuosity must be introduced. Assuming $\tau = 3.6$ this consideration yields for the Vycor pore network $L \approx 1.2\,D$. This result can vividly be interpreted as follows: The shortest way from the bottom of the previously introduced sample cuboid to its top is about 20% longer than its edge length a. With all the preceding considerations in mind one is able to derive an expression that describes the flow of a liquid through a porous network. For a given porous matrix with cross-sectional area A and thickness d (along which the pressure drop Δp is applied) the normalized volume flow rate $\frac{1}{A}\dot{V}$ is determined by

$$\frac{1}{A}\,\dot{V} = \frac{K}{\eta\, d}\,\Delta p. \tag{4}$$

This expression is also known as Darcy's law [91]. The proportionality constant K is the so-called hydraulic permeability of the matrix. It is given by

$$K = \frac{\phi_0}{8\,\tau}\,r_0^2. \tag{5}$$

Note that the permeability is solely specified by the matrix' internal structure and consequently it should be independent of the liquid and of the temperature.

B. Influence of confinement

So far we have completely neglected that the mean pore diameters of the pore network are orders of magnitude smaller than characteristic in usual flow paths in common miniaturized fluid manipulating applications. Indeed, the pore radii are merely 10 to 100 times larger than typical molecular diameters of simple liquids like water. For that reason it is evident that some questions about the influence of the confinement on the fluid dynamics arise. In the following the two most apparent ones will be discussed.

1. Validity of continuum mechanical theory

Unitl now we have assumed the law of Hagen-Poiseuille to be valid even in pores with diameters below 10 nm. However, one must not forget that this law is based on the principles of continuum mechanical theory, in which the behavior of a fluid is determined by collective properties such as the viscosity η and the surface tension σ. This assumption certainly holds for ensembles of 10^{23} molecules. But within the pore confinement such amounts are not reached. Assuming water molecules to be spheres with a radius of 1.5 Å in a hexagonal close-packed structure one arrives at only 1000 molecules per cross-sectional area. As a consequence, the validity of the continuum theory has to be put into question.

On this score especially the development of the SFA has stimulated extensive studies over the past three decades. The mobility of water and several hydrocarbons in extremely confined films was examined by experiment [57,102,103] and in theory [104]. These studies revealed a remarkable robustness of the liquids' fluidity down to nanometer and even subnanometer spatial confinement. Moreover, the validity of macroscopic capillarity conceptions at the mesoscale was demonstrated [48,105–107]. The measurements presented below will provide further hints regarding whether the concepts of viscosity still remain valid in nanopore confinement.

2. Validity of the no-slip boundary condition

The law of Hagen-Poiseuille implies the no-slip boundary condition. This means that the velocity of the fluid layers directly adjacent to the restricting walls equal the velocity of the walls themselves. Nowadays it is indisputable that this assumption does not hold unreservedly. In the 1950s Debye and Cleland introduced both slipping and sticking fluid layers at the pore walls in order to interpret their seminal experiment on liquid flow across porous Vycor [91]. In that way, they were able to quantitatively account both for increased as well as for decreased measured flow rates (compared to the predicted ones) within their examinations of the flow of hydrocarbons through porous Vycor.

The concepts of a sticking and of a slipping liquid compared to the traditional no-slip boundary condition are exemplified in Fig. 2 for a cylindrical tube with radius r_0. The degree of slip can be quantified by the slip length b with $r_0 \equiv r_\mathrm{h} - b$. The hydrodynamic pore radius r_h measures the distance from the pore center to the radius where the streaming velocity reaches zero. In this representation the sticking layer boundary condition is indicated by a negative slip length b, whereas a positive slip length is typical of a slip boundary condition. The standard no-slip condition yields $b = 0$ meaning $r_0 = r_\mathrm{h}$.

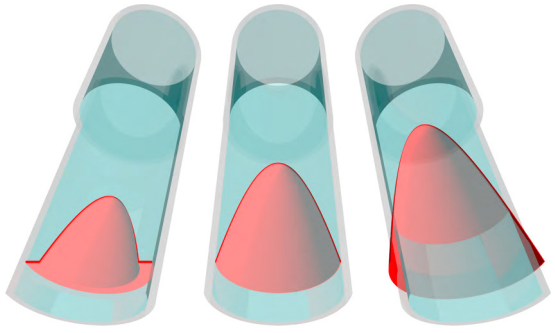

FIG. 2. Illustration of the possible boundary conditions along with the corresponding parabolic velocity profiles in a cylindrical tube with radius r_0. Mass transport takes place only where the streaming velocity differs from zero. Left: The reduction of the net flow rate is due to sticking layers at the pore walls, which do not participate in the mass transport. In addition the maximum velocity in the pore center is smaller than for no-slip boundary conditions (middle) because of the smaller hydrodynamic pore radius $r_\mathrm{h} < r_0$. This gives rise to a further dramatic decrease in the flow rate. Right: In contrast, a slipping liquid with a hydrodynamic pore radius $r_\mathrm{h} > r_0$ causes the highest streaming velocity and, consequently, the highest net flow rate.

Because of the modified boundary conditions one has to substitute r_h for r in Eq. (1). This procedure yields

$$K = \frac{\phi_0}{8\,\tau}\,\frac{r_h^4}{r_0^2} = \frac{\phi_0}{8\,\tau}\,\frac{(r_0+b)^4}{r_0^2} \tag{6}$$

for the permeability of the membrane. Equation (6) illustrates the high sensitivity of K on b, provided b is on the order of or even larger than r_0. Therefore, measuring the hydraulic permeability gives direct access to the slip length b for a given liquid under given conditions.

One has to keep in mind that boundary conditions and fluid properties derived from measured flow rates are subject to a central restriction: One cannot verify the predefined parabolic shape of the velocity profile in the mesoscopic flow geometry. This is because there is no direct access to the profile itself but only to flow rates, which correspond to the velocity profile integrated over the whole pore cross-sectional area. Nevertheless, molecular dynamics simulations prove the formation of parabolic flow profiles even down to channel radii of three molecular diameters [108–110] and, hence, justify inferences based on this major assumption.

C. Forced imbibition

In the case of forced imbibition, where an external pressure is applied to induce liquid flow in a porous medium, the dynamics of the flow through a host of thickness d and cross-sectional area A (that is already completely filled with the liquid) can directly be related to Darcy's law Eq. (4) in conjunction with the permeability K according to Eq. (6). For a pore network with mean pore radius r_0, porosity ϕ_0, and tortuosity τ and with the liquid's viscosity η, in terms of the volume flow rate this finally reads

$$\dot{V} = \underbrace{\frac{A\,\phi_0}{8\,d\,\eta\,\tau}\,\frac{r_h^4}{r_0^2}}_{C_V}\,\Delta p \tag{7}$$

with Δp denoting the (externally generated) pressure drop that is applied along d. By determining the prefactor C_V through a measurement of $\dot{V}(\Delta p)$ the hydrodynamic pore radius r_h is easily accessible.

III. EXPERIMENTAL

A. Materials

The spatial restrictions in the nanometer range were provided by the spongelike topology of porous Vycor glass (Corning, code 7930). Vycor is virtually pure fused silica glass permeated by a three-dimensional network of interconnected, elongated pores [42,111–113]. The experiments were performed with two types of Vycor significantly differing in the mean pore radius $\bar{r}_0$ only, whereas they both coincide in the volume porosity $\phi_0 \approx 0.3$. The aspect ratio a = pore diameter and pore length of Vycor glasses is between 5 and 7 [111–113]. For convenience, the two types will be termed V5 ($\bar{r}_0 = 3.4$ nm) and V10 ($\bar{r}_0 = 5.0$ nm) in the following. The matrix properties have been determined by means of nitrogen sorption isotherms performed at 77 K.

Prior to using, we subjected them to a cleaning procedure with hydrogen peroxide and nitric acid followed by rinsing in deionized Millipore water and drying at 200 °C in vacuum for 2 days. This treatment ensures the removal of any organic contamination on the large internal surface of the samples. Until usage the samples were stored in a desiccator.

The Vycor membranes are highly hydrophilic. This is a consequence of glass being a high-energy surface with chemical binding energies on the order of 1 eV. Nearly any liquid spreads on such surfaces. This behavior can be comprehended considering the Young-Dupré equation [with the indices solid (S), liquid (L), and vapor (V) of the interfacial tension γ and the static contact angle θ_0]

$$\gamma_{SV} = \gamma_{SL} + \gamma_{LV}\,\cos\theta_0\,. \tag{8}$$

The empirical Zisman criterion predicts that any liquid fulfilling $\gamma_{LV} < \gamma_C$ (with the critical surface tension γ_C of the surface) totally wets this surface. For glass it is $\gamma_C \approx 150\,\frac{\mathrm{mN}}{\mathrm{m}}$ [114]. Hence, even highly polarizable liquids like water spread on silica surfaces (meaning $\theta_0 = 0°$).

Moreover, silica substrates provide the simple opportunity to alter the surface chemistry and thereby reduce the surface energy. This can be done by silanization [114]. Prior to silanization the samples were flushed with trichloromethane ($CHCl_3$) several times. In the subsequent step they were exposed to a 1:9 mixture of dimethyldichlorosilane [$Si(CH_3)_2Cl_2$] and trichloromethane for about 2 h. In the presence of dimethyldichlorosilane low-energy methyl (CH_3) groups were substituted for the polar and, consequently, high-energy hydroxyl (OH) groups at the glass surface. Afterwards the samples were again flushed with trichloromethane and methanol several times.

It is important to perform this last step thoroughly since any remainder of dimethyldichlorosilane in the sample potentially reverses the silanization reaction in the presence of water, e.g., from the humidity in the laboratory. In order to further minimize the risk for such a reversal reaction the samples were dried over a stream of dry nitrogen.

The samples were characterized again by means of nitrogen sorption isotherms. They reveal a reduction in the mean pore radius of approximately 4 Å, which is consistent with the thickness of the attached methyl groups at the pore walls [115]. The porosity is likewise reduced. The values are listed in Table I. We will denote the silanized samples sV5 and sV10, respectively.

For the permeability experiments we employed deionized Millipore water and n-hexane with a purity of 99% as delivered from Merck.

B. Hydraulic permeability apparatus

The experimental setup for the forced throughput measurements, the hydraulic permeability apparatus (HPA), is illustrated in Fig. 3. All parts liquid containing are immersed in a water bath, which can be heated up to 80 °C. The

TABLE I. Properties of the silanized Vycor batch as extracted from isotherm measurements.

Sample batch	Mean pore radius r_0	Volume porosity ϕ_0
sV5	(3.0 ± 0.1) nm	0.235 ± 0.02

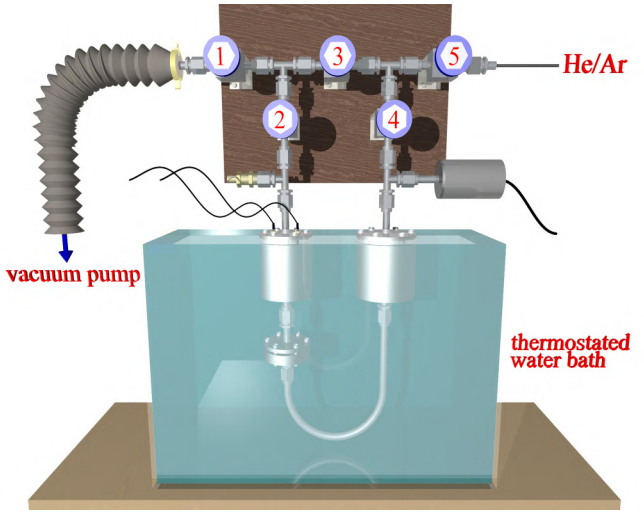

FIG. 3. Ray-tracing illustration of the hydraulic permeability apparatus (HPA) consisting of a gas handling and the actual flow system. The latter is temperature controlled in a water bath. The gas handling can be evacuated by a vacuum pump and can be filled with helium or argon gas.

external pressure is provided by a highly pressurized gas. For this purpose the flow system is connected to a gas handling, which supplies the gas via valves 5 and 4. The valves 1, 2, and 3 permit an initial evacuation of the handling; during the measurements they are normally closed thereby separating the (right) high-pressure side from the (left) low-pressure side. The complete setup is manufactured inhouse and made of stainless steel. This allows for maximum pressures of up to 70 bar, which can be measured with a capacitive pressure transducer. The pressure beyond the capacitor is fixed to the upper limit of 1 bar by means of a blow off valve.

For most measurements the liquid was pressurized with high-purity helium gas (6.0). This choice was made in order to lessen the impact of a major flaw in the measuring method: The liquid stands in direct contact with the highly pressurized gas. Some imaginable consequences will be discussed in the next section. However, with the usage of an inert gas at least chemical reactions can be prevented. What is more, helium is the gas that is, at room temperature, the least soluble in water [116]. In order to study a possible influence of the solubility of the gas on the dynamics argon (purity 5.7) was used as well.

Via the supply channel the pressurized liquid in the reservoir reaches the cell with the cylindrical sample of typically $d = 4$ mm thickness and a diameter of 6 mm. The latter is thoroughly glued into a copper sample holder using the two component, thermally conductive epoxy encapsulant Stycast 2850 with the catalyst 24LV from Emerson and Cuming. With this procedure one must not only accomplish the task of fixing the sample but also that of sealing the sample's side facets in order to guarantee the flow through the top and bottom facets only; or, equivalently, the procedure should ensure that the pressure drop is applied along the complete sample thickness d.

Beyond the sample cell the cylindrical capacitor is attached. Due to the liquid flow through the sample the liquid level in the capacitor rises thereby changing the capacitance. The latter can accurately be ascertained employing a multifrequency

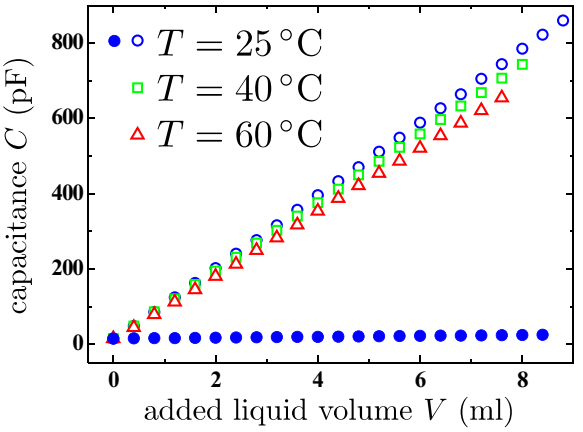

FIG. 4. Calibration measurements of the cylindrical capacitor for water (open symbols) and n-hexane (filled symbols) at selected temperatures. The capacitance C was measured as a function of the liquid amount V filled into the capacitor. For the empty capacitor it is $C \approx 15$ pF.

LCR meter (HP 4275A) at the frequency $f = 500$ kHz. This value was chosen with regard to water's high dielectric loss within the microwave range (roughly between 1 GHz and 1 THz), which would entail additional inaccuracies due to the strong f dependency of the permittivity. For $f = 500$ kHz the dielectric constant only shows the persistent dependence on the temperature T.

For a direct relation between the shift in the capacitance C and the related change in the liquid volume V in the capacitor the latter was calibrated. For this purpose its capacitance was measured while it was stepwise filled with specific amounts of the respective liquid. Since the permittivity is a function of the temperature this procedure was performed for all relevant T. In general, each calibration was repeated at least 5 times. Some of the resultant $C(V)$ curves are exemplarily shown in Fig. 4.

The plots confirm the above-mentioned good applicability of water because of its high dielectric constant as compared with n-hexane. Additionally, the influence of the temperature is clearly recognizable: With increasing T the polarizability decreases due to the enhanced microscopic mobility of the molecules. Macroscopically this behavior is expressed in terms of a decreasing permittivity of the liquid.

One is now able to connect a certain change in C with an equivalent change in V via a calibration factor C_{cal} that is the slope of the shown calibration curves: $\frac{dC}{dV} \equiv C_{\mathrm{cal}}$ [115]. The flow of n-hexane was measured at 50 °C instead of 60 °C (as for water) because of the increasing noise in the proximity of its boiling point at 69 °C.

Using Eq. (7) this finally results in a relationship between the measured variation of the capacitance C as a function of the time t (at a given applied pressure gradient Δp) and the flow dynamics in confinement,

$$\dot{C} = C_{\mathrm{cal}}\,\dot{V} = C_{\mathrm{cal}}\,C_{\mathrm{V}}\,\Delta p, \tag{9}$$

expressed in terms of the prefactor C_{V} [see Eq. (7)]. The most accurate way to deduce C_{V} is to extract the slope of a $\dot{V}(\Delta p) = \frac{\dot{C}(\Delta p)}{C_{\mathrm{cal}}}$ plot.

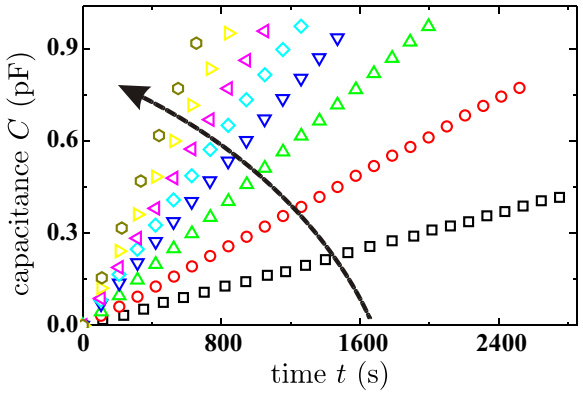

FIG. 5. Time-dependent variation in the capacitance C of the cylinder capacitor due to the flow of water through V10 at 25 °C for a series of applied external pressures. The arrow indicates the direction of increasing Δp. The shown measurements correspond to 8 bar, 16 bar, 24 bar, 31 bar, 37 bar, 45 bar, 54 bar, and 70 bar. The data density is reduced by a factor of 20.

IV. RESULTS AND DISCUSSION

A. Hydraulic transport across hydrophilic Vycor with native silica surfaces

In this first part we will present results obtained from forced throughput measurements on untreated Vycor. The raw data signal of the capacitance change C as a function of the time t is exemplarily shown in Fig. 5 for the flow of water in V10 at $T = 25\,^{\circ}\mathrm{C}$ and for selected applied pressures generated with helium gas. It is evident that with increasing Δp the variation in C with t, that is, the slope $\dot{C}$, increases gradually. This result can directly be interpreted in terms of an increasing volume flow rate $\dot{V} = \frac{\dot{C}}{C_{\mathrm{cal}}}$ with increasing pressure.

In Fig. 6 some of the resultant volume flow rates $\dot{V}$ of water in both V5 and V10 at three different temperatures are plotted

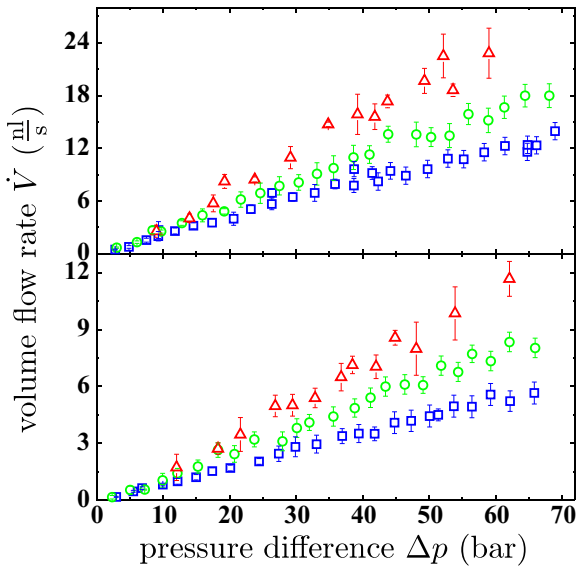

FIG. 6. Volume flow rates $\dot{V}$ of water in V10 (upper panel) and V5 (lower panel) as a function of the applied external pressure difference Δp at three different temperatures: 25 °C (square), 40 °C (circle), and 60 °C (triangle).

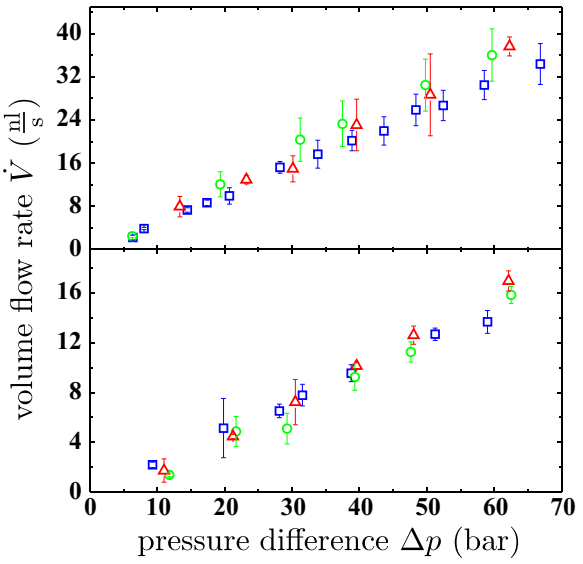

FIG. 7. Volume flow rates $\dot{V}$ of n-hexane in V10 (upper panel) and V5 (lower panel) as a function of the applied external pressure difference Δp at three different temperatures: 25 °C (squares), 40 °C (circle), and 50 °C (triangle).

as a function of the applied external pressure Δp. The same was done for the flow of n-hexane. Some of the corresponding results are shown in Fig. 7. However, due to the rather low calibration factor of n-hexane as compared with that of water, the measuring time had to be increased in order to gain a proper signal with sufficient resolution. For that reason the overall data density is markedly reduced for n-hexane.

In principle all data sets show a linear relation compliant with Eq. (9). The comparison between different temperatures implies—at least for water—a distinct T dependence of the proportionality constant C_{V}: The latter increases with increasing temperature. According to Eq. (7) this behavior is solely determined by the temperature dependence of the liquid's viscosity. Qualitatively this is true: At higher temperatures the lower viscosities cause an increase in C_{V}. But in the temperature region of interest the T dependency of the viscosity of water is more distinctive than that of n-hexane. This behavior renders the effect more pronounced for water.

In a subsequent step the values of the hydrodynamic pore radii r_{h} were calculated from the extracted slopes C_{V}. Based on the matrix properties stated earlier and on the known sample dimensions A and d one arrives at the slip lengths $b = r_{\mathrm{h}} - r_0$ listed in Table II. The error margins in b represent standard deviations. Some of the volume flow rate data do not extrapolate to zero for zero pressure difference. This may result from an underestimation of the error margins and/or systematic errors in the tiny flow rates at small pressure differences, e.g., by small gas leaks in the setup or temperature drifts in the pressure gauges. Along with the error bars in the C_{V} data it results in the comparably large error margins in b. Since the slip lengths should principally be independent of the respective liquid and the measuring temperature they allow for a more quantitative analysis and comparability of the results.

First, nearly all extracted slip lengths are negative, suggesting a sticking layer boundary condition in agreement with

TABLE II. Slip lengths b (in Å) of water and n-hexane flowing through V5 and V10, respectively, as extracted from forced throughput measurements at three different temperatures T (in °C). The liquids were pressurized with helium.

	V5		V10	
T	Water	n-Hexane	Water	n-Hexane
25	-2.6 ± 1.6	-3.8 ± 1.8	-0.1 ± 2.2	-2.8 ± 2.6
40	-1.8 ± 2.1	-4.5 ± 2.2	-0.3 ± 2.9	-1.9 ± 2.9
50		-3.5 ± 2.4		-3.2 ± 2.8
60	-1.3 ± 2.3		0.7 ± 3.6	

previous spontaneous imbibition experiments on water and n-alkanes [92,96,117]. This indicates a compartmentation of the imbibed liquid into (1) an interfacial layer whose dynamics are mainly determined by the interaction between liquid and substrate and (2) an inner (away from the interface) region that shows the classical behavior as predicted from collective liquid properties like viscosity or surface tension. This conclusion is supported by molecular dynamics studies on the glassy structure of water boundary layers in Vycor [118,119] or, more generally, on layering and increased viscosities at silica [120–122] and hydrophilic surfaces [123–127], by structural studies documenting a partitioning of water in a core and a surface water contribution in silica pores [128,129], and by tip-surface measurements in purified water [130]. It is also consistent with beam-bending experiments on water permeability of Vycor [131,132] as well as pecularities in the measured thermal expansion and diffusivities of aquaous solutions confined in Vycor [121,122].

This immobile shell in the case of hexane is in agreement with the pioneering experiments on forced imbibition of n-alkanes by Debye and Cleland [91], mentioned above, as well as experimental and theoretical studies regarding the thinning of n-alkane films in the surface force apparatus [51–55].

Moreover, x-ray reflectivity studies indicate one strongly adsorbed, flat lying monolayer of hydrocarbons on silica [133–136]. Quasielastic neutron-scattering measurements, which are sensitive to the center-of-mass self-diffusion of the n-alkanes in the pores and thus the liquid's viscosity, also indicate a partitioning of the diffusion dynamics of the molecules in the pores in two species: one component with a bulklike self-diffusion dynamics and a second one which is immobile and sticky on the time scale probed in the neutron-scattering experiment [137–140].

However, by means of gravimetrical capillary rise measurements [92,117] and beam-bending experiments [121,131,132], a thickness of the sticky layer of approximately 5 Å and 6 Å, respectively, for water in Vycor were inferred. But the values stated in Table II all deviate towards lower values and eventually b turns even positive for water in V10. For water there seems also to be a marginal increase in b with T, whereas there is no systematic dependency for n-hexane. Contrasting the results for water with the results for n-hexane it turns out that the slip lengths for water are always higher than those for the alkane. Furthermore, the values for V10 are systematically increased as compared with V5.

The bottom line of these results is that the forced imbibition dynamics are generally increased as compared to previously reported spontaneous imbibition experiments [47,92,96,115,117]. Additionally, there are configurations regarding the flowing liquid and the substrate that seemingly facilitate higher slip lengths. This observation can be condensed as follows:

$$b(\text{hexane}) < b(\text{water})$$
$$b(\text{V5}) < b(\text{V10}) .$$

The increase of b with increasing temperature for water is only vague but should not remain unmentioned at this point.

In the forced imbibition measurements the liquid stands in direct contact with the highly pressurized gas. Consequently, it is unavoidable that gas is dissolved in the liquid and thereby possibly influences the flow experiments. It has often been reported that dissolved gas modulates slip [85,86]. For Newtonian fluids enhanced dynamics were found to be consistent with a two-layer-fluid model, in which a layer <1 nm thick, but with viscosity 10–20 times less than the bulk fluid, adjoins each solid surface [78]. A potential mechanism to explain the genesis of this layer was discussed by Vinogradova [141] and formalized by de Gennes [142], who hypothesized that shear may induce nucleation of vapor bubbles; once the nucleation barrier is exceeded the bubbles grow to cover the surface, and the liquid flow takes place over this thin gas film rather than the solid surface itself. Hence, the segregation of gas at the near-surface region seems to facilitate some kind of low-density surface regions, but the nature of these is not understood well at this time.

SFA measurements on tetradecane performed by Granick *et al.* impressively elucidate this theory [85]. The experiments showed that whereas no-slip behavior was obeyed when the tetradecane had been saturated with carbon dioxide gas, massive deviations from this prediction were found when the tetradecane was saturated with argon. Argon possesses only low solubility in tetradecane what may have made it more prone to segregate at the surfaces.

According to these results and considerations the shear rate and the solubility of the gas (hereinafter denoted as $\mathcal{S}$) determine the possible influence of such segregation at a near-surface region. In the following we will assess whether a process like this can be responsible for the observed peculiarities.

First, an impact of the shear rate can indeed be noticed. Since for a given applied pressure difference the maximum shear rate in a channel increases with the fifth power of the channel radius, one may conclude that gas segregation, and therefore enhanced flow dynamics, are more likely in V10 than in V5. This behavior could explain the higher slip lengths in V10 as compared to V5. Note that in the case of water flowing through V10, our data would even be fully compatible with the assumption of $b = 0$. This finding would not be compatible with the assumption that the slip length is solely determined by adsorbed molecular layers and thus by the fluid-wall interactions, since they are identical for both matrices.

A potential effect caused by the gas' solubility in the respective liquid can be assessed considering the solubilities listed in Tables III and IV. It is obvious that for a given

TABLE III. Solubilities $\mathcal{S}$ (in $\frac{\text{mmol}}{\ell}$) of helium and argon in water [116,143] and n-hexane [144–146] at 1 bar for selected temperatures (in °C).

	Helium		Argon	
T	Water	n-Hexane	Water	n-Hexane
20	0.36		1.55	
25		1.98	1.40	19.50
40	0.32	2.40	1.15	18.30
60	0.27		0.94	

temperature the solubility of helium is higher in n-hexane than in water. According to the above-mentioned segregation of gas and the enhanced flow dynamics should be more likely for water than for n-hexane. This prediction coincides with the observed systematically higher slip lengths for water. Even the vague increase in b with the temperature T is consistent with the slight decrease in $\mathcal{S}$ with increasing temperature. Granick's conjecture is in accord with the observed behavior.

For an additional test some forced imbibition experiments in V10 were also carried out with argon instead of helium. According to Table III its solubility in water is about 4 times higher than that of helium; in n-hexane it is even up to 10 times higher. Accordingly, for both experiments one would expect smaller slip lengths as compared to the measurements with helium. For water there is indeed a slight decrease in b; see Table V. Although, for n-hexane the result is rather ambiguous.

Note, however, that the experiments with argon rule out the possibility that the dissolved gas results in an "apparent" b reduction mediated by a decrease in viscosity of the liquid in the pore center by the gas. Upon changing from helium to argon a pronounced viscosity drop and thus increase in b would be expected in this case because of the 10-fold higher solubility of argon in the liquid. However, by contrast, rather, a b decrease is found, in agreement with the smaller tendency for gas separation at the solid-liquid interface.

Of course, important information could be gained from experiments where the fluid is completely separated from the gas, e.g., by a flexible but gas-impermeable membrane. Despite the fact that we tried a variety of flexible membranes with varying chemical constitution, we always noticed a final gas permeability. Still, for the future it would be interesting to compare experiments with and without such membranes. A sizable reduction of the gas dissolution could in particular be possible for argon, since for the large argon atom (in comparison to helium) flexible membranes with smaller gas permeability are available, e.g., based on polyvinylidene chloride [147]. However, already the experiments by Debye and Cleland [91] are in this respect an important reference for the present study, since they performed forced imbibition studies on native

TABLE IV. Solubilities $\mathcal{S}$ (in $\frac{\text{mmol}}{\ell}$) of helium in water at 25 °C for selected pressures p (in bar) [143].

p	1	3	5	7.5	10	25	50	75
$\mathcal{S}$	0.36	1.09	1.77	2.7	3.53	8.78	17.5	26.3

TABLE V. Slip lengths b (in Å) of water and n-hexane flowing through V10 pressurized by two different gases, namely helium (He) and argon (Ar).

Liquid	Temperature	He	Ar
Water	25 °C	-0.1 ± 2.2	-1.2 ± 3.3
n-Hexane	25 °C	-2.8 ± 2.6	-2.3 ± 3.1
	40 °C	-1.9 ± 2.9	-1.6 ± 3.5

Vycor glass without the application of pressurized gases. In agreement with the spontaneous imbibition experiments discussed above, they found a smaller slip length for n-hexane in V10 than in our experiments performed under inert gas pressure, i.e., $b = -5$ Å. Hence, also a comparison with their experiments corroborates our considerations with regard to a gas-dissolution-induced increase in hydraulic permeability of Vycor glass.

B. Hydraulic transport across hydrophobic Vycor with silanized silica surfaces

As outlined in the Introduction the high significance of the liquid-substrate interaction in restricted geometries has been pointed out several times so far. In particular, the boundary conditions are markedly influenced by the wettability of the substrate [63–71]. This encourages measurements on the flow dynamics through porous Vycor with a modified surface chemistry.

The results from the measurements on silanized Vycor compared to the values from the respective untreated sample are shown in Table VI in terms of slip lengths. The value for water in sV5 is not available since even for the highest pressures applied (70 bar) no flow through the sample could be detected. Contrary to this collapse in the dynamics of water the flow of n-hexane seems to have been even enhanced.

It is obvious that the modified surface chemistry of the porous Vycor samples significantly influences the dynamics of both liquids. Some basic discoveries are in high accordance with an NMR study of water and several alcohols in similarly treated Vycor glass [148]. The inability of water to penetrate the sV5 sample must be traced back to the modified wettability of the substrate. Spontaneous imbibition could be observed for neither sV5 nor sV10. In consequence, a capillary depression caused by a contact angle $\theta_0 > 90°$ is substituted for the capillary rise mechanism. One can estimate a lower bound for θ_0 from the finding that even pressures up to 70 bar cannot

TABLE VI. Slip lengths b (in Å) of water and n-hexane flowing through untreated and surface silanized Vycor, respectively. The liquids were pressurized with helium.

System	Temperature	Untreated	Silanized
Water in (s)V5	25 °C	-2.6 ± 1.6	n/a
Hexane in (s)V5	25 °C	-3.8 ± 1.8	0.3 ± 2.7
	40 °C	-4.5 ± 2.2	0.4 ± 2.8
	50 °C	-3.5 ± 2.4	0.4 ± 3.8

overcome the counteracting Laplace pressure:

$$\cos\theta_0 < -\frac{\Delta p\, r_0}{2\,\sigma}\,, \tag{10}$$

thus it is $\theta_0 > 98^\circ$. Depending on the actual methyl density of the silanized surface, water can have contact angles up to 120° corresponding to a Laplace pressure of ∼240 bar. Therefore, the complete blocking of water penetration of the sV5 sample is not surprising at all [149]. It is rather a preeminent elucidation of the magnitude of surface forces.

The results on the flow of *n*-hexane in sV5 (the same sample that was used in the water experiment) can be explained by the reduction of the surface energy of Vycor due to silanization. It weakens the attractive interaction between the surface and the alkane. This is expressed by the distinct disappearance of the sticking layer in favor of a classical no-slip boundary condition although, according to the Zisman criterion, the liquid should still totally wet the surface.

V. CONCLUSIONS

To summarize, we performed experiments on the pressure-driven flow of water and *n*-hexane across monolithic nanoporous Vycor. The hydraulic flow rates can be rationalized if one assumes a negative velocity slip length, i.e., a sticking molecular layer. The thickness of this layer is thinner than inferred from spontaneous imbibition experiments. This observation is traced to an increased slippage at the pore wall resulting from the partial dissolution of the gases used to drive the flows. Moreover, we verified that the wettability of the substrate deeply influences the flow dynamics and boundary conditions. The observed effects range from increasing slip lengths for *n*-hexane to complete blocking of the flow for water. Especially for the alkane we observe that, by silanization of the pore wall, we can achieve a vanishing of the sticking boundary layer.

For the future, the study of longer alkanes, which possess higher surface tensions, would permit more detailed examinations of the influence of the wettability. Also experiments on silanized samples with larger pore diameter than examined here are planned, since they should allow us to overcome the pressure barrier for water flow in the pores and thus to study water transport in hydrophobic pores. Furthermore, the surface coating with fluorinated groups (instead of methyl groups) causes reductions of the critical surface tension down to $\sim 6\,\frac{\mathrm{mN}}{\mathrm{m}}$ [114]. By these means the interplay of surface wettability (solid-liquid interactions) and confinement and its impact on flow at the continuum limit could be further explored [40].

ACKNOWLEDGMENTS

This work was supported by the German Science Foundation (DFG) within the priority program 1164, "Nano- & Microfluidics" (Grant No. Hu 850/2) and within the Collaborative Research Initiative SFB 986, "Tailor-Made Multi-Scale Materials Systems," research area B, Hamburg.

[1] J. C. T. Eijkel and A. van den Berg, Nanofluidics: What is it and what can we expect from it? Microfluid. Nanofluid. **1**, 249 (2005).

[2] A. D. Stroock, Vinay V. Pagay, M. A. Zwieniecki, and N. M. Holbrook, The physicochemical hydrodynamics of vascular plants, Annu. Rev. Fluid Mechan. **46**, 615 (2014).

[3] M. Mastrangeli, The fluid joint: The soft spot of micro- and nanosystems, Adv. Mater. **27**, 4254 (2015).

[4] D. T. Birdsell, H. Rajaram, D. Dempsey, and H. S. Viswanathan, Hydraulic fracturing fluid migration in the subsurface: A review and expanded modeling results, Water Resour. Res. **51**, 7159 (2015).

[5] K. Falk, B. Coasne, R. Pellenq, F.-J. Ulm, and L. Bocquet, Subcontinuum mass transport of condensed hydrocarbons in nanoporous media, Nat. Commun. **6**, 6949 (2015).

[6] A. J. Yin, J. Li, W. Jian, A. J. Bennett, and J. M. Xu, Fabrication of highly ordered metallic nanowire arrays by electrodeposition, Appl. Phys. Lett. **79**, 1039 (2001).

[7] A. Huczko, Template-based synthesis of nanomaterials, Appl. Phys. A **70**, 365 (2000).

[8] M. Steinhart, J. H. Wendorff, A. Greiner, R. B. Wehrspohn, K. Nielsch, J. Schilling, J. Choi, and U. Gosele, Polymer nanotubes by wetting of ordered porous templates, Science **296**, 1997 (2002).

[9] M. S. Sander and L. S. Tan, Nanoparticle arrays on surfaces fabricated using anodic alumina films as templates, Adv. Funct. Mater. **13**, 393 (2003).

[10] P. E. de Jongh and T. M. Eggenhuisen, Melt infiltration: An emerging technique for the preparation of novel functional nanostructured materials, Adv. Mater. **25**, 6672 (2013).

[11] P. Huber, Soft matter in hard confinement: Phase transition thermodynamics, structure, texture, diffusion and flow in nanoporous media, J. Phys. Condens. Matter **27**, 103102 (2015).

[12] H. Pleinert, H. Sadouki, and F. H. Wittmann, Determination of moisture distributions in porous building materials by neutron transmission analysis, Mater. Struct. **31**, 218 (1998).

[13] W. Vichit-Vadakan and G. W. Scherer, Measuring permeability of rigid materials by a beam-bending method: Iii, cement paste, J. Am. Ceram. Soc. **85**, 1537 (2002).

[14] Xiaojiang Zhang, Yinghong Qiao, Lina Xu, and Lian M. Buriak, Constructing metal-based structures on nanopatterned etched silicon, ACS Nano **5**, 5015 (2011).

[15] I. Rosenhek-Goldian, N. Kampf, A. Yeredor, and J. Klein, On the question of whether lubricants fluidize in stick-slip friction, Proc. Natl. Acad. Sci. USA **112**, 7117 (2015).

[16] A. Y. Jee, K. Lou, and S. Granick, Scrutinizing evidence of no dilatancy upon stick-slip of confined fluids, Proc. Natl. Acad. Sci. USA **112**, E4972 (2015).

[17] J. N. Israelachvili and C. Drummond, On the conformational state of molecules in molecularly thin shearing films, Proc. Natl. Acad. Sci. USA **112**, E4973 (2015).

[18] M. Michelin-Jamois, C. Picard, G. Vigier, and E. Charlaix, Giant Osmotic Pressure in the Forced Wetting of Hydrophobic Nanopores, Phys. Rev. Lett. **115**, 036101 (2015).
[19] B. Lefevre, A. Saugey, J. L. Barrat, L. Bocquet, E. Charlaix, P. F. Gobin, and G. Vigier, Intrusion and extrusion of water in highly hydrophobic mesoporous materials: Effect of the pore texture, Colloids Surf. A **241**, 265 (2004).
[20] Y. Grosu, O. Ievtushenko, V. Eroshenko, J. M. Nedelec, and J. P. E. Grolier, Water intrusion/extrusion in hydrophobized mesoporous silica gel in a wide temperature range: Capillarity, bubble nucleation and line tension effects, Colloids Surf. A **441**, 549 (2014).
[21] V. D. Borman, A. A. Belogorlov, A. M. Grekhov, and V. N. Tronin, States of a dispersed nonwetting liquid in a disordered nanoporous medium, Int. J. Mod. Phys. B **29**, 1550097 (2015).
[22] H. A. Stone, A. D. Stroock, and A. Ajdari, Engineering flows in small devices: Microfluidics toward a laboratory-on-a-chip, Annu. Rev. Fluid Mechan. **36**, 381 (2004).
[23] T. M. Squires and S. R. Quake, Microfluidics: Fluid physics at the nanoliter scale, Rev. Mod. Phys. **77**, 977 (2005).
[24] M. Majumder, N. Chopra, R. Andrews, and B. J. Hinds, Enhanced flow in carbon nanotubes, Nature **438**, 44 (2005).
[25] P. S. Dittrich and A. Manz, Lab-on-a-chip: Microfluidics in drug discovery, Nat. Rev. Drug Discovery **5**, 210 (2006).
[26] M. Whitby and N. Quirke, Fluid flow in carbon nanotubes and nanopipes, Nat. Nanotechnol. **2**, 87 (2007).
[27] R. Karnik, K. Castelino, C. Duan, and A. Majumdar, Diffusion-limited patterning of molecules in nanofluidic channels, Nano Lett. **6**, 1735 (2006).
[28] F. Persson, L. H. Thamdrup, M. B. L. Mikkelsen, S. E. Jaarlgard, P. Skafte-Pedersen, H. Bruus, and A. Kristensen, Double thermal oxidation scheme for the fabrication of SiO_2 nanochannels, Nanotechnology **18**, 245301 (2007).
[29] R. B. Schoch, J. Han, and P. Renaud, Transport phenomena in nanofluidics, Rev. Mod. Phys. **80**, 839 (2008).
[30] M. Muller, C. Pastorino, and J. Servantie, Flow, slippage and a hydrodynamic boundary condition of polymers at surfaces, J. Phys. Condens. Matter **20**, 494225 (2008).
[31] A. Piruska, M. Gong, J. V. Sweedler, and P. W. Bohn, Nanofluidics in chemical analysis, Chem. Soc. Rev. **39**, 1060 (2010).
[32] B. J. Kirby, *Micro- and Nanoscale Fluid Mechanics: Transport in Microfluidic Devices* (Cambridge University Press, Cambridge, 2010).
[33] L. Bocquet and E. Charlaix, Nanofluidics, from bulk to interfaces, Chem. Soc. Rev. **39**, 1073 (2010).
[34] S. Koester and T. Pfohl, X-ray studies of biological matter in microfluidic environments, Mod. Phys. Lett. B **26**, 1230018 (2012).
[35] C. Duan, W. Wang, and Q. Xie, Review article: Fabrication of nanofluidic devices, Biomicrofluidics **7**, 026501 (2013).
[36] L. Bocquet and P. Tabeling, Physics and technological aspects of nanofluidics, Lab Chip **14**, 3143 (2014).
[37] O. Vincent, D. A. Sessoms, E. J. Huber, J. Guioth, and A. D. Stroock, Drying by cavitation and poroelastic relaxations in porous media with macroscopic pores connected by nanoscale throats, Phys. Rev. Lett. **113**, 134501 (2014).
[38] Y. Xue, Switchable imbibition in nanoporous gold, Nat. Commun. **5**, 4237 (2014).
[39] M. Tani, R. Kawano, K. Kamiya, and K. Okumura, Towards combinatorial mixing devices without any pumps by open-capillary channels: Fundamentals and applications, Sci. Rep. **5**, 10263 (2015).
[40] O. Vincent, A. Szenicer, and A. Stroock, Capillarity-driven flows at the continuum limit, arXiv:1510.00411.
[41] L. Li, J. Mo, and Z. Li, Nanofluidic Diode for Simple Fluids Without Moving Parts, Phys. Rev. Lett. **115**, 134503 (2015).
[42] P. Huber and K. Knorr, Adsorption-desorption isotherms and x-ray diffraction of Ar condensed into a porous glass matrix, Phys. Rev. B **60**, 12657 (1999).
[43] L. D. Gelb, K. E. Gubbins, R. Radhakrishnan, and M. Sliwinska-Bartkowiak, Phase separation in confined systems, Rep. Prog. Phys. **62**, 1573 (1999).
[44] H. K. Christenson, Confinement effects on freezing and melting, J. Phys. Condens. Matter **13**, R95 (2001).
[45] C. Alba-Simionesco, B. Coasne, G. Dosseh, G. Dudziak, K. E. Gubbins, R. Radhakrishnan, and M. Sliwinska-Bartkowiak, Effects of confinement on freezing and melting, J. Phys. Condens. Matter **18**, R15 (2006).
[46] K. Knorr, P. Huber, and D. Wallacher, Thermodynamic and structural investigations of condensates of small molecules in mesopores, Z. Phys. Chem. **222**, 257 (2008).
[47] S. Gruener and P. Huber, Imbibition in mesoporous silica: rheological concepts and experiments on water and a liquid crystal, J. Phys. Condens. Matter **23**, 184109 (2011).
[48] C. Fradin, A. Braslau, D. Luzet, D. Smilgies, M. Alba, N. Boudet, K. Mecke, and J. Daillant, Reduction in the surface energy of liquid interfaces at short length scales, Nature **403**, 871 (2000).
[49] O. I. Vinogradova and A. V. Belyaev, Wetting, roughness and flow boundary conditions, J. Phys. Condens. Matter **23**, 184104 (2011).
[50] O. Bäumchen, L. Marquant, R. Blossey, A. Münch, B. Wagner, and K. Jacobs, Infuence of Slip on the Rayleigh-Plateau Rim Instability in Dewetting Viscous Films, Phys. Rev. Lett. **113**, 014501 (2014).
[51] D. Y. C. Chan and R. G. Horn, The drainage of thin liquid-films between solid-surfaces, J. Chem. Phys. **83**, 5311 (1985).
[52] H. K. Chirstenson, R. G. Horn, and J. N. Israelachvili, Measurement of forces due to structure in hydrocarbon liquids, J. Colloid Interface Sci. **88**, 79 (1982).
[53] M. J. Stevens, M. Mondello, G. S. Grest, S. T. Cui, H. D. Cochran, and P. T. Cummings, Comparison of shear flow of hexadecane in a confined geometry and in bulk, J. Chem. Phys. **106**, 7303 (1997).
[54] J. M. Georges, S. Millot, J. L. Loubet, and A. Tonck, Drainage of thin liquid-films between relatively smooth surfaces, J. Chem. Phys. **98**, 7345 (1993).
[55] U. Heinbuch and J. Fischer, Liquid flow in pores: Slip, no-slip, or multilayer sticking, Phys. Rev. A **40**, 1144 (1989).
[56] M. Ruths and S. Granick, Influence of alignment of crystalline confining surfaces on static forces and shear in a liquid crystal, 4′-*n*-pentyl-4-cyanobiphenyl, Langmuir **16**, 8368 (2000).
[57] U. Raviv, P. Laurat, and J. Klein, Fluidity of water confined to subnanometre films, Nature **413**, 51 (2001).
[58] C. Neto, D. R. Evans, E. Bonaccurso, H. J. Butt, and V. S. J. Craig, Boundary slip in Newtonian liquids: A review of experimental studies, Rep. Prog. Phys. **68**, 2859 (2005).

[59] J. Harting, C. Kunert, and J. Hyvaluoma, Lattice boltzmann simulations in microfluidics: Probing the no-slip boundary condition in hydrophobic, rough, and surface nanobubble laden microchannels, Microfluid. Nanofluid. **8**, 1 (2010).
[60] O. Baeumchen and K. Jacobs, Slip effects in polymer thin films, J. Phys. Condens. Matter **22**, 033102 (2010).
[61] C. Chen, L. Zhuang, X. F. Li, J. F. Dong, and J. T. Lu, A many-body dissipative particle dynamics study of forced water-oil displacement in capillary, Langmuir **28**, 1330 (2012).
[62] M. Sedghi, M. Piri, and L. Goual, Molecular dynamics of wetting layer formation and forced water invasion in angular nanopores with mixed wettability, J. Chem. Phys. **141**, 194703 (2014).
[63] J. L. Barrat and L. Bocquet, Large Slip Effect at a Nonwetting Fluid-Solid Interface, Phys. Rev. Lett. **82**, 4671 (1999).
[64] R. Pit, H. Hervet, and L. Leger, Direct Experimental Evidence of Slip in Hexadecane: Solid Interfaces, Phys. Rev. Lett. **85**, 980 (2000).
[65] M. Cieplak, J. Koplik, and J.R. Banavar, Boundary Conditions at a Fluid-Solid Interface, Phys. Rev. Lett. **86**, 803 (2001).
[66] D. C. Tretheway and C. D. Meinhart, Apparent fluid slip at hydrophobic microchannel walls, Phys. Fluids **14**, L9 (2002).
[67] Jae-Hie J. Cho, B. M. Law, and F. Rieutord, Dipole-Dependent Slip of Newtonian Liquids at Smooth Solid Hydrophobic Surfaces, Phys. Rev. Lett. **92**, 166102 (2004).
[68] T. Schmatko, H. Hervet, and L. Leger, Friction and Slip at Simple Fluid-Solid Interfaces: The Roles of the Molecular Shape and the Solid-Liquid Interaction, Phys. Rev. Lett. **94**, 244501 (2005).
[69] R. Fetzer and K. Jacobs, Slippage of Newtonian liquids: Influence on the dynamics of dewetting thin films, Langmuir **23**, 11617 (2007).
[70] R. S. Voronov, D. V. Papavassiliou, and L. L. Lee, Review of fluid slip over superhydrophobic surfaces and its dependence on the contact angle, Ind. Eng. Chem. Res. **47**, 2455 (2008).
[71] A. Maali, T. Cohen-Bouhacina, and H. Kellay, Measurement of the slip length of water flow on graphite surface, Appl. Phys. Lett. **92**, 053101 (2008).
[72] J. Servantie and M. Müller, Temperature Dependence of the Slip Length in Polymer Melts at Attractive Surfaces, Phys. Rev. Lett. **101**, 026101 (2008).
[73] B. Y. Cao, J. Sun, M. Chen, and Z. Y. Guo, Molecular momentum transport at fluid-solid interfaces in mems/nems: A review, Int. J. Mol. Sci. **10**, 4638 (2009).
[74] T. A. Ho, D. V. Papavassiliou, L. L. Lee, and A. Striolo, Liquid water can slip on a hydrophilic surface, Proc. Natl. Acad. Sci. USA **108**, 16170 (2011).
[75] D. Schaeffel, S. Yordanov, M. Schmelzeisen, T. Yamamoto, M. Kappl, R. Schmitz, B. Dünweg, H.-J. Butt, and K. Koynov, Hydrodynamic boundary condition of water on hydrophobic surfaces, Phys. Rev. E **87**, 051001(R) (2013).
[76] R. Bhadauria and N. R. Aluru, A quasi-continuum hydrodynamic model for slit shaped nanochannel flow, J. Chem. Phys. **139**, 074109 (2013).
[77] P. A. Thompson and S. M. Troian, A general boundary condition for liquid flow at solid surfaces, Nature **389**, 360 (1997).
[78] Y. Zhu and S. Granick, Rate-Dependent Slip of Newtonian Liquid at Smooth Surfaces, Phys. Rev. Lett. **87**, 096105 (2001).
[79] V. S. J. Craig, C. Neto, and D. R. M. Williams, Shear-Dependent Boundary Slip in an Aqueous Newtonian Liquid, Phys. Rev. Lett. **87**, 054504 (2001).
[80] N. V. Priezjev and S. M. Troian, Molecular Origin and Dynamic Behavior of Slip in Sheared Polymer Films, Phys. Rev. Lett. **92**, 018302 (2004).
[81] N. V. Priezjev, Rate-dependent slip boundary conditions for simple fluids, Phys. Rev. E **75**, 051605 (2007).
[82] O. I. Vinogradova and G. E. Yakubov, Surface roughness and hydrodynamic boundary conditions, Phys. Rev. E **73**, 045302(R) (2006).
[83] Y. Zhu and S. Granick, Limits of the Hydrodynamic No-Slip Boundary Condition, Phys. Rev. Lett. **88**, 106102 (2002).
[84] E. Bonaccurso, H. J. Butt, and V. S. J. Craig, Surface Roughness and Hydrodynamic Boundary Slip of a Newtonian Fluid in a Completely Wetting System, Phys. Rev. Lett. **90**, 144501 (2003).
[85] S. Granick, Y. X. Zhu, and H. Lee, Slippery questions about complex fluids flowing past solids, Nat. Mater. **2**, 221 (2003).
[86] S. M. Dammer and D. Lohse, Gas Enrichment at Liquid-Wall Interfaces, Phys. Rev. Lett. **96**, 206101 (2006).
[87] T. H. Yen, Molecular dynamics simulation of fluid containing gas in hydrophilic rough wall nanochannels, Microfluid. Nanofluid. **17**, 325 (2014).
[88] C. Cheikh and G. Koper, Stick-Slip Transition at the Nanometer Scale, Phys. Rev. Lett. **91**, 156102 (2003).
[89] E. Lauga and T. M. Squires, Brownian motion near a partial-slip boundary: A local probe of the no-slip condition, Phys. Fluids **17**, 103102 (2005).
[90] M. E. Nordberg, Properties of some vycor-brand glasses, J. Am. Ceram. Soc. **27**, 299 (1944).
[91] P. Debye and R. L. Cleland, Flow of liquid hydrocarbons in porous Vycor, J. Appl. Phys. **30**, 843 (1959).
[92] S. Gruener, T. Hofmann, D. Wallacher, A. V. Kityk, and P. Huber, Capillary rise of water in hydrophilic nanopores, Phys. Rev. E **79**, 067301 (2009).
[93] B. Abeles, L. F. Chen, J. W. Johnson, and J. M. Drake, Capillary condensation and surface flow in microporous vycor glass, Isr. J. Chem. **31**, 99 (1991).
[94] S. Gruener and P. Huber, Knudsen Diffusion in Silicon Nanochannels, Phys. Rev. Lett. **100**, 064502 (2008).
[95] S. Gruener, Z. Sadjadi, H. E. Hermes, A. V. Kityk, K. Knorr, S. U. Egelhaaf, H. Rieger, and P. Huber, Anomalous front broadening during spontaneous imbibition in a matrix with elongated pores, Proc. Natl. Acad. Sci. USA **109**, 10245 (2012).
[96] S. Gruener, Helen E. Hermes, B. Schillinger, S. U. Egelhaaf, and P. Huber, Capillary rise dynamics of liquid hydrocarbons in mesoporous silica as explored by gravimetry, optical and neutron imaging: Nano-rheology and determination of pore size distributions from the shape of imbibition fronts, Colloids Surf. A (2015).
[97] M. Alava, M. Dube, and M. Rost, Imbibition in disordered media, Adv. Phys. **53**, 83 (2004).
[98] D. I. Dimitrov, A. Milchev, and K. Binder, Forced imbibition—A tool for separate determination of Laplace pressure and drag force in capillary filling experiments, Phys. Chem. Chem. Phys. **10**, 1867 (2008).

[99] M. Y. Lin, B. Abeles, J. S. Huang, H. E. Stasiewski, and Q. Zhang, Visocus Flow and Diffusion of Liquids in Microporous Glasses, Phys. Rev. B **46**, 10701 (1992).
[100] S. Bommer, Gas- und Proteinpermeabilitätsmessungen an biomimetischen Festkörpermembranen, Ph.D. thesis, Saarland University, Saarbrücken, Germany, 2008.
[101] R. A. Crossley, L. M. Schwartz, and J. R. Banavar, Image-based models of porous media: Application to Vycor glass and carbonate rocks, Appl. Phys. Lett. **59**, 3553 (1991).
[102] J. Israelachvili, Measurement of the viscosity of liquids in very thin films, J. Colloid Interface Sci. **110**, 263 (1986).
[103] R. G. Horn, D. T. Smith, and W. Haller, Surface forces and viscosity of water measured between silica sheets, Chem. Phys. Lett. **162**, 404 (1989).
[104] S. A. Gupta, H. D. Cochran, and P. T. Cummings, Shear behavior of squalane and tetracosane under extreme confinement. III. Effect of confinement on viscosity, J. Chem. Phys. **107**, 10335 (1997).
[105] L. R. Fisher, R. A. Gamble, and J. Middlehurst, The Kelvin equation and the capillary condensation of water, Nature **290**, 575 (1981).
[106] D. Seveno, T. D. Blake, and J. De Coninck, Young's Equation at the Nanoscale, Phys. Rev. Lett. **111**, 096101 (2013).
[107] J. Landers, G. Y. Gor, and A. V. Neimark, Density functional theory methods for characterization of porous materials, Colloids Surf. A **437**, 3 (2013).
[108] B. D. Todd and D. J. Evans, The heat-flux vector for highly inhomogeneous nonequilibrium fluids in very narrow pores, J. Chem. Phys. **103**, 9804 (1995).
[109] K. P. Travis, B. D. Todd, and D. J. Evans, Departure from navier-stokes hydrodynamics in confined liquids, Phys. Rev. E **55**, 4288 (1997).
[110] D. I. Dimitrov, A. Milchev, and K. Binder, Capillary Rise in Nanopores: Molecular Dynamics Evidence for the Lucas-Washburn Equation, Phys. Rev. Lett. **99**, 054501 (2007).
[111] P. Levitz, G. Ehret, S.K. Sinha, and J. M. Drake, Porous Vycor glass: The microstructure as probed by electron microscopy, direct energy transfer, small-angle scattering, and molecular adsorption, J. Chem. Phys. **95**, 6151 (1991).
[112] A. C. Mitropoulos, J. M. Haynes, R. M. Richardson, and N. K. Kanellopoulos, Characterization of porous glass by adsorption of dibromomethane in conjunction with small-angle x-ray scattering, Phys. Rev. B **52**, 10035 (1995).
[113] L. D. Gelb and K. E. Gubbins, Characterization of porous glasses: Simulation models, adsorption isotherms, and the Brunauer-Emmett-Teller analysis method, Langmuir **14**, 2097 (1998).
[114] P. G. de Gennes, F. Brochard-Wyart, and D. Quere, *Capillarity and Wtting Phenomena: Drops, Bubbles, Pearls, Waves* (Springer, New York, 2004).
[115] S. Gruener, Rheology and dynamics of simple and complex liquids in mesoporous matrices, Ph.D. thesis, Saarland University, Saarbrücken, Germany, 2010.
[116] R. W. Potter and M. A. Clynne, The solubility of the noble gases He, Ne, Ar, Kr, and Xe in water up to the critical point, J. Solution Chem. **7**, 837 (1978).
[117] S. Gruener and P. Huber, Spontaneous Imbibition Dynamics of an n-alkane in Nanopores: Evidence of Meniscus Freezing and Monolayer Sticking, Phys. Rev. Lett. **103**, 174501 (2009).
[118] P. Gallo, M. Rovere, and E. Spohr, Glass transition and layering effects in confined water: A computer simulation study, J. Phys. Chem. **113**, 11324 (2000).
[119] P. A. Bonnaud, B. Coasne, and R. J. M. Pellenq, Molecular simulation of water confined in nanoporous silica, J. Phys. Condens. Matter **22**, 284110 (2010).
[120] D. Argyris, N. R. Tummala, A. Striolo, and D. R. Cole, Molecular structure and dynamics in thin water films at the silica and graphite surfaces, J. Phys. Chem. C **112**, 13587 (2008).
[121] S. Xu, G. C. Simmons, T. S. Mahadevan, G. W. Scherer, S. H. Garofalini, and C. Pacheco, Transport of water in small pores, Langmuir **25**, 5084 (2009).
[122] S. Xu, G. W. Scherer, T. S. Mahadevan, and S. H. Garofalini, Thermal expansion of confined water, Langmuir **25**, 5076 (2009).
[123] Ch. Sendner, D. Horinek, L. Bocquet, and R. R. Netz, Interfacial water at hydrophobic and hydrophilic surfaces: Slip, viscosity, and diffusion, Langmuir **25**, 10768 (2009).
[124] D. Jan Bonthuis, S. Gekle, and R. R. Netz, Profile of the static permittivity tensor of water at interfaces: Consequences for capacitance, hydration interaction and ion adsorption, Langmuir **28**, 7679 (2012).
[125] T. Q. Vo, M. Barisik, and B. H. Kim, Near-surface viscosity effects on capillary rise of water in nanotubes, Phys. Rev. E **92**, 053009 (2015).
[126] R. Bhadauria, T. Sanghi, and N. R. Aluru, Interfacial friction based quasi-continuum hydrodynamical model for nanofluidic transport of water, J. Chem. Phys. **143**, 174702 (2015).
[127] B. Kim, S. Kwon, M. Lee, Q. Kim, S. An, and W. Jhe, Probing nonlinear rheology layer-by-layer in interfacial hydration water, Proc. Nat. Acad. Sci. (USA) **112**, 15619 (2015).
[128] M. C. Bellissent-Funel, Status of experiments probing the dynamics of water in confinement, Eur. Phys. J. E **12**, 83 (2003).
[129] M. Erko, N. Cade, A. G. Michette, G. H. Findenegg, and O. Paris, Confinement-induced structural changes of water studied by Raman scattering, Phys. Rev. B **84**, 104205 (2011).
[130] T. D. Li, J. Gao, R. Szoszkiewicz, U. Landman, and E. Riedo, Structured and viscous water in subnanometer gaps, Phys. Rev. B **75**, 115415 (2007).
[131] G. W. Scherer, Measuring permeability of rigid materials by a beam-bending method: I, theory, J. Am. Ceram. Soc. **83**, 2231 (2000).
[132] W. Vichit-Vadakan and G. W. Scherer, Measuring permeability of rigid materials by a beam-bending method: Ii, porous glass, J. Am. Ceram. Soc. **83**, 2240 (2000).
[133] S. Basu and S. K. Satija, In-situ x-ray reflectivity study of alkane films grown from the vapor phase, Langmuir **23**, 8331 (2007).
[134] H. D. Mo, G. Evmenenko, and P. Dutta, Ordering of liquid squalane near a solid surface, Chem. Phys. Lett. **415**, 106 (2005).
[135] M. Bai, K. Knorr, M. J. Simpson, S. Trogisch, H. Taub, S. N. Ehrlich, H. Mo, U. G. Volkmann, and F. Y. Hansen, Nanoscale observation of delayering in alkane films, Europhys. Lett. **79**, 26003 (2007).
[136] T. P. Corrales, M. Bai, V. del Campo, P. Homm, P. Ferrari, A. Diama, Ch. Wagner, H. Taub, K. Knorr, M. Deutsch, M. J. Retamal, U. G. Volkmann, and P. Huber, Spontaneous formation of nanopatterns in velocity-dependent dip-coated

organic films: From dragonflies to stripes, ACS Nano **8**, 9954 (2014).

[137] J. Baumert, B. Asmussen, C. Gutt, and R. Kahn, Pore-size dependence of the self-diffusion of hexane in silica gels, J. Chem. Phys. **116**, 10869 (2002).

[138] A. Kusmin, S. Gruener, A. Henschel, O. Holderer, J. Allgaier, D. Richter, and P. Huber, Evidence of a sticky boundary layer in nanochannels: A neutron spin echo study of *n*-hexatriacontane and poly(ethylene oxide) confined in porous silicon, J. Phys. Chem. Lett. **1**, 3116 (2010).

[139] A. Kusmin, S. Gruener, A. Henschel, N. de Souza, J. Allgaier, D. Richter, and P. Huber, Polymer dynamics in nanochannels of porous silicon: A neutron spin echo study, Macromolecules **43**, 8162 (2010).

[140] Tommy Hofmann, Dirk Wallacher, Maria Mayorova, Reiner Zorn, Bernhard Frick, and Patrick Huber, Molecular dynamics of *n*-hexane: A quasi-elastic neutron scattering study on the bulk and spatially nanochannel-confined liquid, J. Chem. Phys. **136**, 124505 (2012).

[141] O. I. Vinogradova, Slippage of water over hydrophobic surfaces, Int. J. Miner. Process. **56**, 31 (1999).

[142] P. G. de Gennes, On fluid/wall slippage, Langmuir **18**, 3413 (2002).

[143] V. I. Baranenko, L. N. Falkovskii, V. S. Kirov, Y. V. Filimonov, Y. E. Lebedev, A. N. Musienko, and A. I. Piontkovskii, Solubility of helium in water, At. Energ. **66**, 407 (1989).

[144] A. E. Markham and K. A. Kobe, The solubility of gases in liquids, Chem. Rev. **28**, 519 (1941).

[145] H. L. Clever, R. Battino, J. H. Saylor, and P. M. Gross, The solubility of helium, neon, argon and krypton in some hydrocarbon solvents, J. Phys. Chem. **61**, 1078 (1957).

[146] P. J. Hesse, R. Battino, P. Scharlin, and E. Wilhelm, Solubility of gases in liquids, J. Chem. Eng. Data **41**, 195 (1996).

[147] L. K. Massey, *Permeability Properties of Plastics and Elastomers* (Elsevier, Amsterdam, 2002).

[148] Y. Hirama, T. Takahashi, M. Hino, and T. Sato, Studies of water adsorbed in porous Vycor glass, J. Colloid Interface Sci. **184**, 349 (1996).

[149] E. R. Cruz-Chu, A. Aksimentiev, and K. Schulten, Water-silica force field for simulating nanodevices, J. Phys. Chem. B **110**, 21497 (2006).